Isothermal Crystallization and Melting of Isotactic Polypropylene Analyzed by Time- and Temperature-Dependent Small-Angle X-ray Scattering Experiments

M. Iijima† and G. Strobl*

Fakultät für Physik der, Albert-Ludwigs-Universität, 79104 Freiburg, Germany

Received January 6, 2000; Revised Manuscript Received April 27, 2000

ABSTRACT: Structure evolution during isothermal crystallization of isotactic polypropylene and the changes during a subsequent heating to the melt were analyzed by time- and temperature-dependent small-angle X-ray scattering experiments. Results demonstrate that isotactic polypropylene, when forming the α-polymorph, is governed by the same general laws for crystallization and melting as syndiotactic polypropylene. Crystal thicknesses are inversely proportional to the supercooling under a characteristic temperature T_c^∞ which is located above the equilibrium melting point of a sample. The crystallization line describing this dependence can be understood as representing the stability limit of a well-defined initial state with higher free energy. Its transformation into the final lamellar two-phase structure provides the stabilization expressed in the difference between the crystallization and melting temperature. Observations and data from other sources can be seen as indicating that (i) crystal thicknesses are independent of the isotacticity and that (ii) the initial state is composed of crystal blocks in planar assemblies, in agreement with corresponding observations on syndiotactic polypropylene. The small-angle X-ray scattering experiments provide a detailed insight into the structure changes during the continuous melting. For high crystallization temperatures no recrystallization occurs. Crystals with different stabilities, all having the same thickness, melt consecutively. Structures produced at low crystallization temperatures are less stable. Here heating leads to repeated melting−recrystallization processes associated with jumplike changes in the length scale of the structure.

1. Introduction

Structure formation during crystallization of isotactic polypropylene (iPP) includes some peculiarities and is therefore more complex than for the majority of other standard polymers. (A recent review by Bicerano[1] provides an overview and includes also an extensive list of references.) Briefly one observes the following special features: (i) In addition to the stable monoclinic α-form one finds metastable β- and γ-polymorphs. Their occurrence, usually as a minority component, depends on the chosen crystallization temperature and the isotacticity and can also be modified by the inclusion of co-units. (ii) Even for most rapid quenches of the melt to temperatures below the glass transition around 0 °C one does not succed to produce a homogeneous perfectly amorphous glass. One rather ends up in a mesophase addressed by many authors as "smectic".[2,3] (iii) As a unique feature one finds crosshatching. Spherulites of i-PP include in addition to radially growing lamellae a second set of transverse layerlike crystallites which are oriented in a perpendicular direction.

Even if these general morphological features are known and in parts also well understood, in particular the occurrence of the set of transverse crystallites as arising from an epitaxial mechanism (Lotz and Wittmann[4]), it remains a difficult matter to analyze for a given sample the crystallization and melting processes. Ideally this requires a combination of different techniques: transmission electron microscopy (TEM) and atomic force microscopy (AFM) to learn about the general morphology, wide-angle X-ray scattering (WAXS) and optical microscopy to detect and distinguish the different polymorphs and to estimate the amount of crosshatching, differential scanning calorimetry (DSC) to register the global changes of the crystallinity during crystallization and melting, and small-angle X-ray scattering (SAXS) to determine the thicknesses of the crystallites and amorphous layers. Over the years there appeared many publications, and they demonstrate a general tendency. It is found that with increasing crystallization temperature the fraction of the stable α-polymorph increases, and the crosshatching frequency becomes smaller. This is mostly true; however, more closer looks also show limitations. For example, one finds after the first weakening of the dominance of the α-phase with decreasing crystallization temperature at low temperatures again an increase,[5] or one observes a coming back of the crosshatches at high crystallization temperatures if the isotacticity is near to perfect.[6]

For syndiotactic polypropylene (s-PP) crystallization behavior is much more simple; there is no competition between different polymorphs and no crosshatching. We used this system in a comprehensive study of crystallization and melting, employing time- and temperature-dependent small-angle X-ray scattering. Experiments yielded accurate results for the relation between the crystallization temperature T_c, the crystallite thickness d_c, and the melting point of the lamellae T_f.[7] The results completely changed our views about the basic processes controlling polymer crystallization. Plots of the temperatures T_f and T_c versus the inverse crystal thickness yield two linear dependencies: the crystallization line T_c versus d_c^{-1} and the Gibbs−Thomson melting line T_f versus d_c^{-1}, and they cross each other at a finite d_c. We understand the existence of the two different dependencies as being indicative for a two-step process when forming the layerlike crystallites, beginning with the

† On leave from Tokyo Medical University, Japan.
* To whom correspondence should be addressed.

10.1021/ma000019m CCC: $19.00
Published on Web 06/14/2000

formation of an initial structure with lower crystalline order which then becomes stabilized to end up in the final crystalline lamellae. The crystallization line is the signature of the initial and the melting line that of the final structure. When studying a series of syndiotactic poly(propene-*co*-octene)s, we found systematic shifts of the melting lines to lower temperatures with increasing octene content but no effect at all on the crystallization line, i.e., on d_c. Following the investigations on s-PP, we examined also poly(ethylene-*co*-octene)s and poly-ϵ-caprolactone.[8] In all cases we observed the same general scenario, with well-defined different crystallization and melting lines which cross each other at a finite value of the crystal thickness.

In the following we present and discuss the results of analogous time- and temperature-dependent SAXS experiments carried out for two different samples of isotactic polypropylene. The higher complexity of the system becomes evident in the obtained data; the evaluation is less straightforward and not from the beginning unambiguous. However, as will be shown, consideration of all the data together yields results that look reliable. The general tendencies come out clearly. Again, the existence of a crystallization line and a melting line expressing different physical dependencies is demonstrated, and both can be determined with reasonable accuracy. Hence, for isotactic polypropylene building up of the lamellar crystallites also passes over an initial form. Experiments provide detailed information about the physical background of the structured DSC curves, and they set up bounds for the equilibrium melting point of perfect i-PP.

2. Experimental Section

2.1. Materials. Two samples of isotactic polypropylene were investigated. Sample iPP1 was synthesized in the Institute of Macromolecular Chemistry of our university using a metallocene catalyst. According to an NMR analysis it has more than 0.98 isotactic pentades (the concentration of regio defects, which might also be present[9] has not been determined); number- and weight-averaged molecular weights are M_n = 32 000 and M_w = 56 000. The second sample iPP2 was a commercially available material supplied by Hoechst AG, Frankfurt (code PPN1060). It has a similar isotacticity as iPP1, but a higher molecular weight, with M_n = 60 000 and M_w = 174 000.

2.2. Instrumentation. The SAXS experiments were carried out with the aid of a Kratky camera attached to a conventional Cu−Kα X-ray source using a temperature-controlled sample holder. Employing a position-sensitive metal wire detector, scattering curves were usually registered within a few minutes counting time. A special algorithm developed in our group was applied in order to deconvolute the slit-smeared scattering data.[10] To remove all memory effects, samples were kept in the melt at 200 °C for more than 1 h before starting an experiment. The cooling to the chosen crystallization temperature was carried out as quickly as possible, typically within 2−3 min. By observation of the intensity it was ensured that crystallization did not start before reaching isothermal conditions.

Complementary wide-angle X-ray scattering experiments (WAXS) were mostly conducted employing a Siemens D500 diffractometer in our lab and in one case at the synchrotron radiation source HASYLAB in Hamburg.

For the registration of DSC thermograms we used a Perkin-Elmer DSC 4. Weight fraction crystallinities were derived from the heat of fusion by taking the ratio to the ideal value ΔH_{id} of a fully crystalline sample. We selected ΔH_{id} = 207 J g^{-1} as determined by Cheng et al.[11]

2.3. SAXS Data Analysis. For stacks of laterally extended layerlike crystallites, the scattering intensity can be related to the one-dimensional electron density correlation function $K(z)$ defined as

$$K(z) = \langle(\rho_e(z) - \langle\rho_e\rangle)(\rho_e(0) - \langle\rho_e\rangle)\rangle = \langle\rho_e(z)\,\rho_e(0)\rangle - \langle\rho_e\rangle^2 \quad (1)$$

It follows from the scattering cross section per unit volume $\Sigma(q)$ as

$$K(z) = \frac{1}{r_e^2}\frac{1}{(2\pi)^3}\int_0^\infty \cos qz\; 4\pi q^2 \Sigma(q)\, dq \quad (2)$$

where q denotes the scattering vector

$$q = \frac{4\pi}{\lambda}\sin\Theta \quad (3)$$

where Θ is the Bragg scattering angle and r_e is the classical electron radius.

A trajectory along the surface normal passes through amorphous regions with an electron density $\rho_{e,a}$ and crystallites with a core density $\rho_{e,c}$. As shown by Ruland,[12] for such a layer system the second derivative of the correlation function, $K''(z)$, gives the distribution of distances between interfaces, in the form

$$K''(z) = \frac{O_{ac}}{2}\Delta\rho_e^2[h_a(z) + h_c(z) - 2h_{ac}(z) \ldots] \quad (4)$$

h_a and h_c give the distributions of the thickness of the amorphous and the crystalline layers, respectively, h_{ac} that of the sum of both, identical with the long spacing L, etc.

If the boundaries between the crystalline and the amorphous regions are sharp within the resolution limit of SAXS experiments, the asymptotic behavior of $\Sigma(q)$ is given by Porod's law

$$\lim_{q\to\infty}\Sigma(q) = r_e^2\frac{P}{(q/2\pi)^4} \quad (5)$$

The Porod coefficient P is directly related to the specific internal surface O_{ac}, i.e., the area per unit volume of the interface separating crystalline and amorphous regions, by

$$P = \frac{1}{8\pi^3}O_{ac}\Delta\rho_e^2 \quad (6)$$

P shows also up in the slope of the triangular part of $K(z)$ as

$$P = \frac{1}{4\pi^3}\frac{dK}{dz} \quad (7)$$

Transition zones at the lamellar surfaces may lead to deviations from Porod's law in the range of the highest accessible scattering angles, but eq 7 remains unaffected. To be sure about possible perturbing effects of transition zones, one should always compare the directly deduced P with that obtained by eq 7. For the samples under study we found always a good agreement.

One may wonder whether the one-dimensional analysis may be applied in the given case where two stacks of lamellae interpenetrate each other. This is in fact possible, since each stack or even each crystallite retains its layerlike form. The interpenetration of the radial and transverse sets of lamellae does not change the situation; one still has an isotropic distribution of stacks of layers. There is only one special effect. Intersection of two layers creates an edge along the intersection line. As was shown in a previous paper,[13] this changes the properties of K'' at q = 0. Without edges, which is the normal situation, one has $K''(0)$ = 0, whereas the occurrence

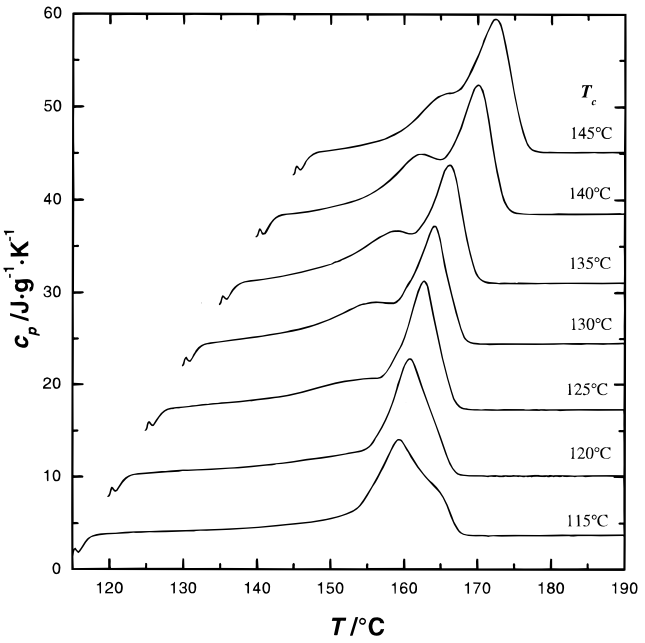

Figure 1. iPP1: DSC melting curve measured after isothermal crystallizations at the indicated temperatures (heating rate: 10 K min^{-1}).

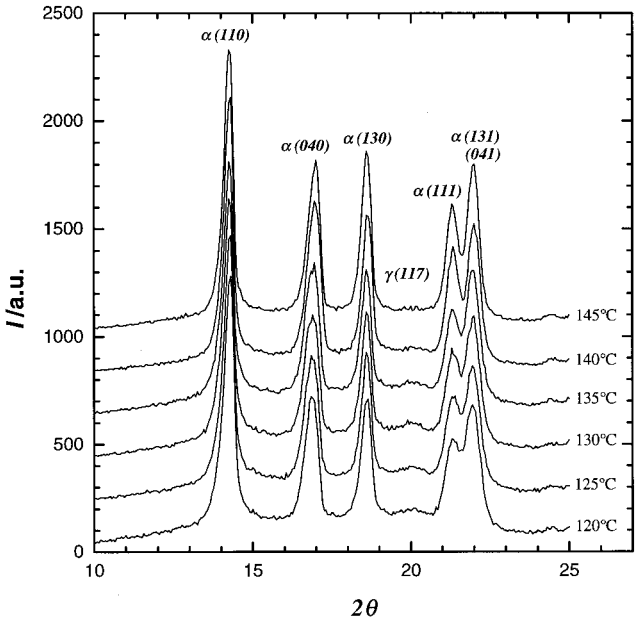

Figure 2. iPP1: WAXS diagrams with assigned reflections obtained after completion of isothermal crystallizations at the indicated temperatures (Θ: Bragg scattering angle).

of edges results in a nonvanishing $K''(0)$. The form of K'' away from the origin remains unchanged.

3. Results and Discussion

3.1. Insights from SAXS and DSC. Figure 1 depicts for sample iPP1 the DSC thermograms measured during heating runs immediately after the completion of isothermal crystallizations at the indicated temperatures (heating rate: 10 K min^{-1}). One observes a systematic shift of the main endothermal peak to higher temperatures with increasing T_c. For crystallization temperatures above 125 °C a second broad endotherm develops on the low-temperature side of the main peak; for the lowest temperatures, 115 and 120 °C, a shoulder comes up on the high temperature side. The latter is obviously due to a recrystallization after a first complete melting. The endothermal contribution on the low-temperature side, in particular the second peak, indicates that the sample includes crystallites with varying stability. DSC curves such as those shown in this figure have been often observed and reported on.

The total heat of melting obtained by integration of the excess heat over the full temperature range is essentially constant. For T_c = 125 °C one finds 128 J g^{-1} and for 145 °C, 134 J g^{-1}, which implies a weight fraction crystallinity $\phi_w = 0.63 \pm 0.01$.

Figure 2 shows WAXS diagrams measured at the different T_c's after completion of the crystallization. They were measured to check for the presence of polymorphs different from the α-form. One finds some indication for the presence of the γ-polymorph as indicated by the characteristic 117-reflection;[14] however, this is really negligible.

To learn in more detail about the building up of the semicrystalline structure and the changes accompanying the heating to the melt, time- and temperature-dependent SAXS experiments were carried out. For T_c = 145 °C a clear picture arose, and this is shown in Figure 3. The lower part depicts on the left the evolution of the interface distance distribution function and on the right-hand side the simultaneous change of the

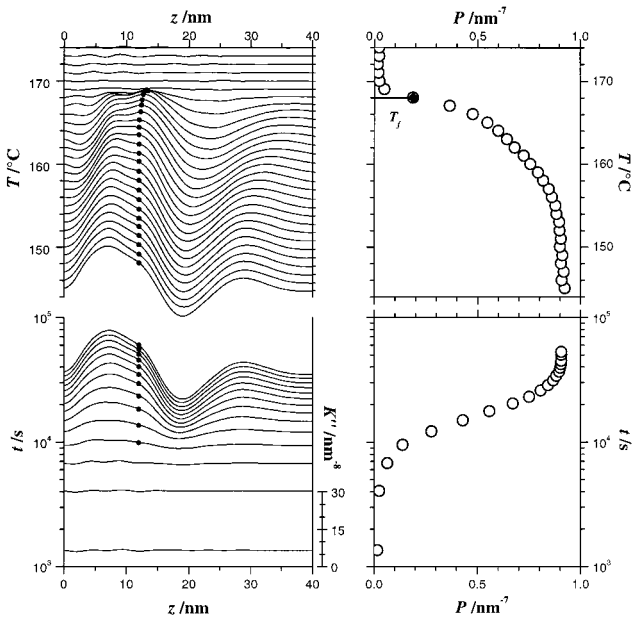

Figure 3. iPP1: evolution of the interface distance distribution function $K''(z)$ during an isothermal crystallization at 145 °C (bottom left) and changes during a subsequent heating to the melt (top left). Related changes of the Porod coefficient (right).

Porod coefficient. The upper part refers to the structure variations during the heating, again showing on the left the changes in K'' and on the right the changes in P. The interface distance distribution function shows two peaks, located at 7 and 12 nm, and a minimum corresponding to the long spacing at 19 nm. As the crystallinity is above 0.5, the assignment is clearly d_a = 7 nm, d_c = 12 nm; this also gives a linear crystallinity $\phi_l = d_c/L \approx 0.63$, in agreement with the DSC value. According to the meaning of $K''(z)$, the peak locations, at d_a and d_c, give the most probable thicknesses. As shown by the curves, this (most probable) crystal thickness remains essentially constant, during both the isothermal crystallization and the subsequent heating. Melting

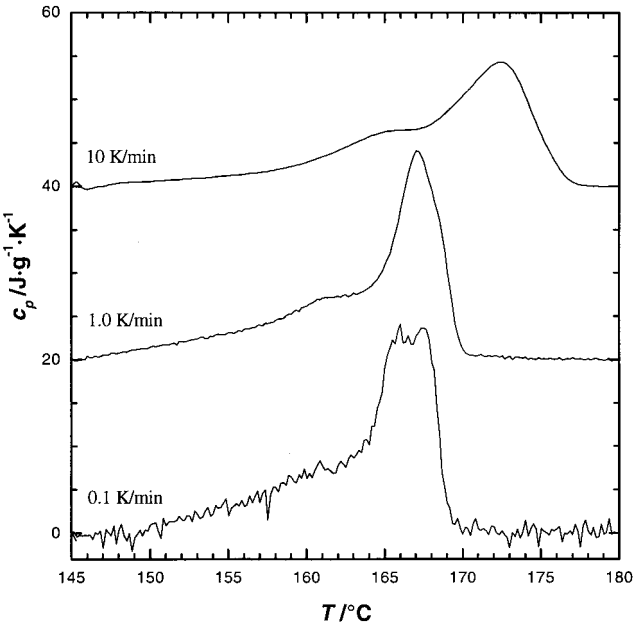

Figure 4. iPP1: thermograms obtained in measurements with different heating rates after an isothermal crystallization at 145 °C.

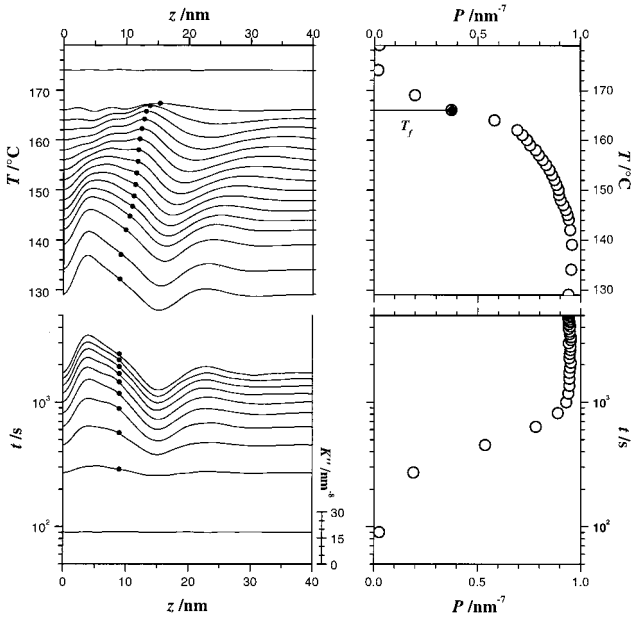

Figure 5. iPP1: evolution of the interface distance distribution function $K''(z)$ during an isothermal crystallization at 130 °C (bottom left) and changes during a subsequent heating to the melt (top left). Related changes of the Porod coefficient (right).

begins immediately at T_c, since the Porod coefficient would increase with temperature due to the increasing electron density difference $\Delta\rho_e$ if the crystallinity would remain constant. According to the temperature dependence of $P(T)$, melting passes through three different regions, with changes around 156 and 165 °C. At the beginning one may note a weak shoulder around 4 nm. This feature has completely disappeared at the end of the first region. In the next temperature range, one observes a decrease in the amplitude of the peaks at 7 and 12 nm, whereby the one associated with the amorphous layers is more affected than that associated with d_c. Around 165 °C the main region of melting begins, showing the highest melting rate at $T_f = 168$ °C. This point, which is especially indicated in the plot, is taken as T_f.

One might expect that T_f agrees with the location of the DSC melting peak. However, there is a clear difference: one finds the DSC peak at 173 °C, shifted up by 5 °C. The origin of the shift becomes apparent when looking for the effect of the heating rate, and this is shown in Figure 4. We employed three different heating rates, the highest one being that used in the thermograms of Figure 1 and the lowest one, 0.1 K min^{-1}, roughly corresponding to the effective heating rate in the temperature-dependent SAXS experiments (10−30 min per measurement, 1 °C temperature steps). There is a remarkably large shift in the location of the main endotherm with the heating rate, and it amounts to the same value as found in the difference between the DSC and the SAXS experiment. Obviously one encounters here a pronounced superheating effect, the same one as reported in a recent paper by Huang et al.[9] It either could arise from the slow response of the DSC or could represent a real effect of the sample. The observations of Alamo et al., that the high-temperature endotherm completely disappears on annealing the sample in between the low- and the high-temperature endotherm, speaks more in favor of a true physical effect.

Melting up to and over the main endotherm takes place at a constant value of d_c. There is no indication at all for recrystallization processes. Obviously crystallites are just removed from the stack. As the removal of one crystallite leads to the disappearance of two amorphous layers, it is also clear why the effect on the d_a peak located at 7 nm is stronger than for the d_c peak.

Isothermal crystallization at $T_c = 145$ °C thus gives clear, unambiguous results. In fact, this is not generally the case. Crystallization and melting of i-PP can be much more complex and the data less clear, and this is demonstrated by the next example in Figure 5. It deals with an analogous representation of the data with the isothermal crystallization at 130 °C and a subsequent heating. The structure evolution during the crystallization is now dominated by a well-defined peak at a rather low distance, 4 nm, a broader peak located at 9 nm, and a minimum in the interface distance distribution function giving the long spacing at 15 nm. Taking into account that the crystallinity is around 60%, we may assign the broad peak at 9 nm to the crystal thickness. The strong peak at 4 nm is at the same location as a weak shoulder in the Figure 3 and has now become a dominant feature. Apparently, it covers the contribution of the amorphous layers expected around 6 nm when taking the difference between the long spacing and d_c. In fact, the d_a peak then shows up at temperatures around 155 °C, where the 4 nm peak has disappeared.

The semicrystalline structure resulting from the crystallization at this lower temperature is much less stable. Different from the behavior found for $T_c = 145$ °C, one now observes a shift of d_c with temperature, and the points marking the positions of d_c depict this dependence. Obviously the melting is now followed immediately by a recrystallization. A first melting occurs around 145 °C, and interestingly, recrystallization then produces crystals of 12 nm thickness, in agreement with those resulting from a direct crystallization at 145 °C. The crystals formed by the recrystallization process at 145 °C remain stable up to 165 °C, just as in the previous example. Hence, both samples end up at the same T_f. However, now comes a difference

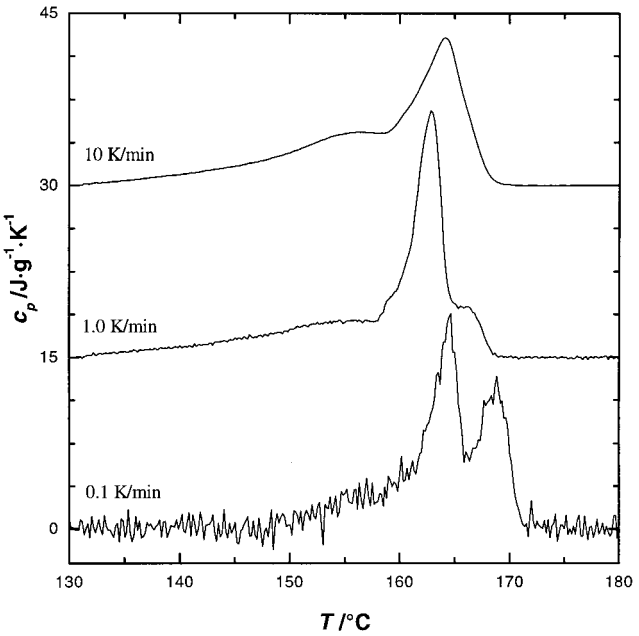

Figure 6. iPP1: thermograms obtained in measurements with different heating rates after an isothermal crystallization at 130 °C.

again. For $T_c = 145$ °C melting was completed just above T_f, while now it extends over another 8 °C. The SAXS experiment shows the reason: Melting is for a second time followed by a recrystallization, at least for some part of the crystallites, which now produces lamellae with a thickness $d_c = 16$ nm.

The recrystallization after the main melting peak is confirmed by the DSC, as is demonstrated by the thermograms given in Figure 6. At the heating rate of the SAXS experiment, 0.1 K min^{-1}, we observe two peaks associated with the first and the second melting. There is a change in the relative weights of the peaks on increasing the heating rate to 1 K min^{-1}, and finally, for 10 K min^{-1}, recrystallization no more occurs. The melting peak, now located at 164 °C, represents the melting of the original lamellae grown at 130 °C. The proof will be given later, when discussing the content of Figure 12.

As the last result presented for sample iPP1, Figure 7 collects all interface distance distribution functions obtained at the various T_c's after completion of the crystallization process. The tendencies showing up in the curves seem to be clear. The locations of the contributions of the crystal thicknesses are marked by points, and those of the long spacings are given by the minima. Both lengths decrease as expected with decreasing crystallization temperature, whereby their ratio remains essentially constant, $d_c/L \approx 0.6$. The contribution of the amorphous layers, d_a, is visible for 150 and 145 °C and located around 7 nm. Then, at lower temperatures, this broad peak is covered by the arising peak at 4 nm.

What does the latter mean? There is no final answer. One knows that with decreasing temperature the cross-hatching tendency becomes more pronounced. It therefore would look conceivable in some way to assign it to the stacks of transverse crystallites. Principally, the peak could either represent amorphous intercrystalline layers or the crystallites themselves. Regarding the values of the measured crystal thicknesses, it appears improbable that the much lower 4 nm length also relates

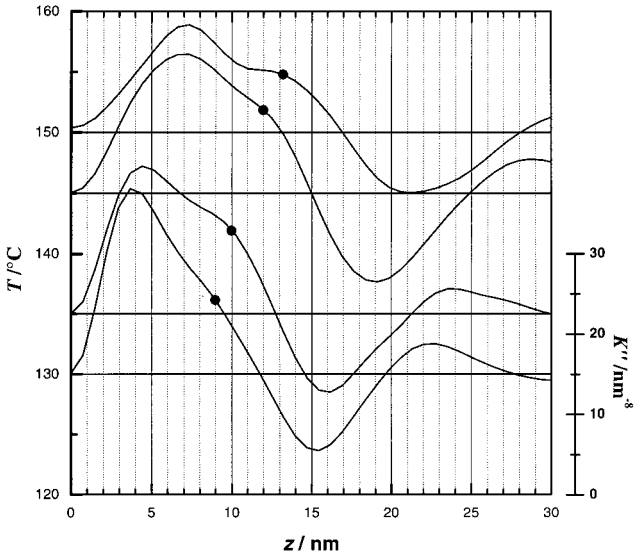

Figure 7. iPP1: interface distribution functions after completion of isothermal crystallizations at 130, 135, 145, and 150 °C.

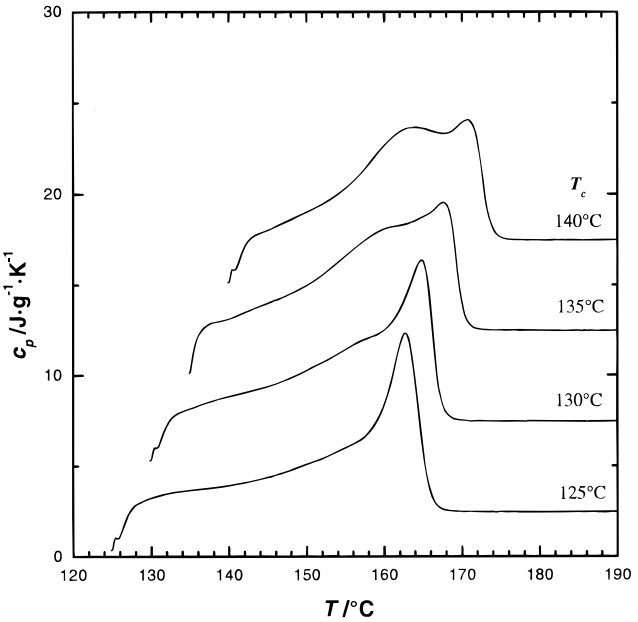

Figure 8. iPP2: DSC melting curve measured after isothermal crystallizations at the indicated temperatures (heating rate: 10 K min^{-1}).

to a crystal. One might suspect, therefore, that the peak represents the smallest possible thickness of the amorphous layers, arising primarily between the transverse lamellae. In fact, Bassett et al.[15] observed this kind of distance between adjacent crystallites in their TEM micrographs, although for both radial and transverse ones.

Measurements for the second sample, iPP2, were carried out in analogous manner and covered a similar temperature range. Figure 8 shows a series of thermograms obtained during heatings immediately after isothermal crystallization processes at the indicated temperatures. Again one observes a systematic shift of the main endotherm to higher temperatures with increasing T_c. Even more, the locations agree with those found for iPP1. There is also a second broad endotherm at the low-temperature side, showing up at the higher T_c's. Different from the first sample there is no indica-

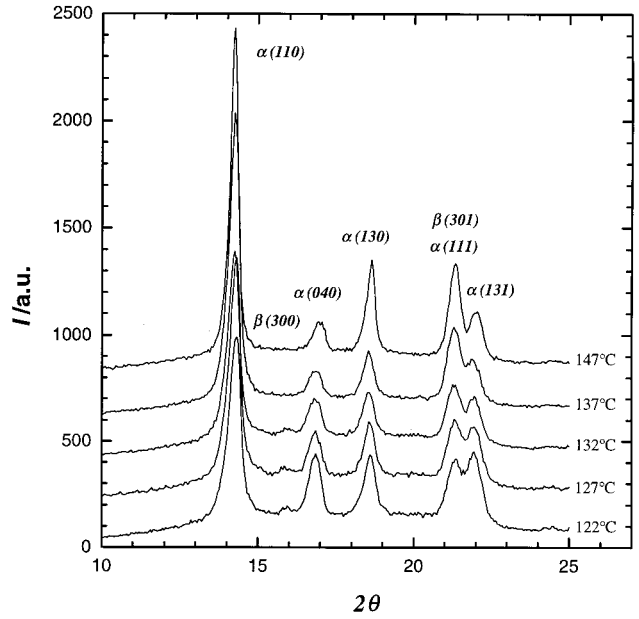

Figure 9. iPP2: WAXS diagrams with assigned reflections obtained after completion of isothermal crystallizations at the indicated temperatures (Θ: Bragg scattering angle).

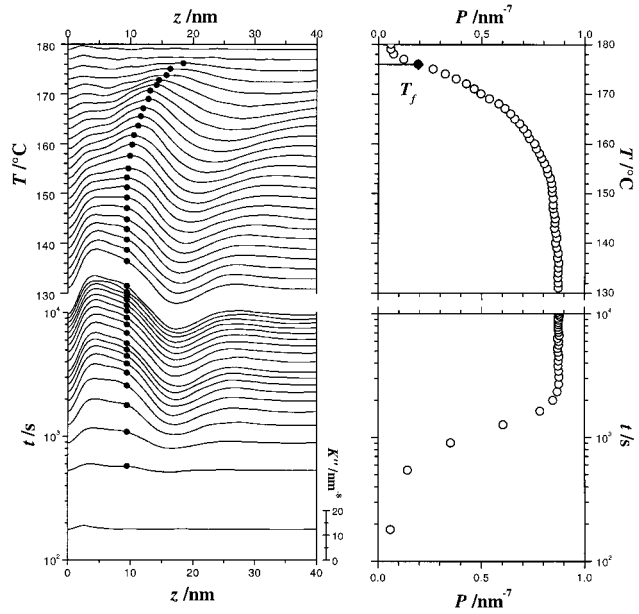

Figure 10. iPP2: evolution of the interface distance distribution function during an isothermal crystallization at 130 °C (bottom left) and changes during a subsequent heating to the melt (top left). Related changes of the Porod coefficient (right).

tion of a recrystallization following the main melting. Measured heats of fusion change from 104 J g^{-1} for the lowest T_c to 110 J g^{-1} for the highest T_c, thus indicating a weight fraction crystallinity of $\phi_w = 0.51 \pm 0.01$. Hence, sample iPP2 has the lower crystallinity, probably a consequence of the higher molecular weight. Figure 9 shows WAXS diagrams registered at the different crystallization temperatures. Again we have an indication for the presence of a second polymorph, but now it is the β-form and again this contribution looks unimportant (when referring to the characteristic peak at $2\theta = 16$ °C).

Figure 10 presents the results of a time- and temperature-dependent SAXS study, as an example the one

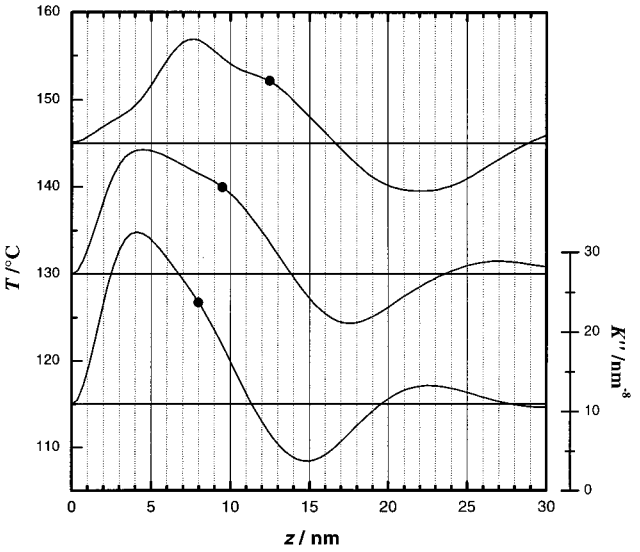

Figure 11. iPP2: interface distribution functions after completion of isothermal crystallizations at 115, 130, and 145 °C.

carried out for $T_c = 130$ °C. It is instructive to compare these results with those obtained for iPP1 at the same T_c depicted in Figure 5. The long spacing amounts to 17 nm, which is somewhat larger than for iPP1; the crystal thickness is found at a similar location, $d_c = 9$ nm. The contribution of the amorphous layers does not show up separately, which is conceivable considering that the crystallinity is around 50%, as is also confirmed by the linear crystallinity. A prominent feature is again the peak at 4 nm, tentatively assigned to the cross-hatches.

The semicrystalline structure of iPP2 seems to be more stable than the one produced at the same T_c for iPP1. The shift of the peak indicating a melting−recrystallization process now occurs around 155 °C, i.e., at a 10 °C higher temperature. Also, the final melting is shifted up, the main melting peak being located at $T_f = 175$ °C. According to the K'' curves registered at this temperature, it relates to a melting of crystallites with a thickness of 18 nm. Hence, heating is accompanied by two melting−recrystallization processes, taking place around 155 and 165 °C and leading in both cases to a steplike increase of d_c. Note that at 155 °C the peak at 4 nm has already disappeared.

We carried out this kind of measurements on iPP2 at three different crystallization temperatures. Figure 11 shows the interface distance distribution functions obtained after completion of the crystallization process. The changes in the long spacing and in the location of the crystal thickness and/or the thickness of the amorphous regions show up quite clearly. The 4 nm peak is visible for the lower temperatures only and is practically absent for $T_c = 145$ °C.

The results obtained for this sample are comparable to those reported by Ryan et al.[16] for a presumably similar i-PP. These authors also observed a constant thickness during the crystallization and then an increase on heating.

3.2. Crystallization Line, Melting Line, and Crystallinity. The SAXS data yielded for both samples the relationship between T_c and d_c and provided information about the dependence of the melting point on the lamellar thickness. As in all previous investigations, we represent the two dependencies in one common plot, giving T_c and T_f as a function of the inverse crystal

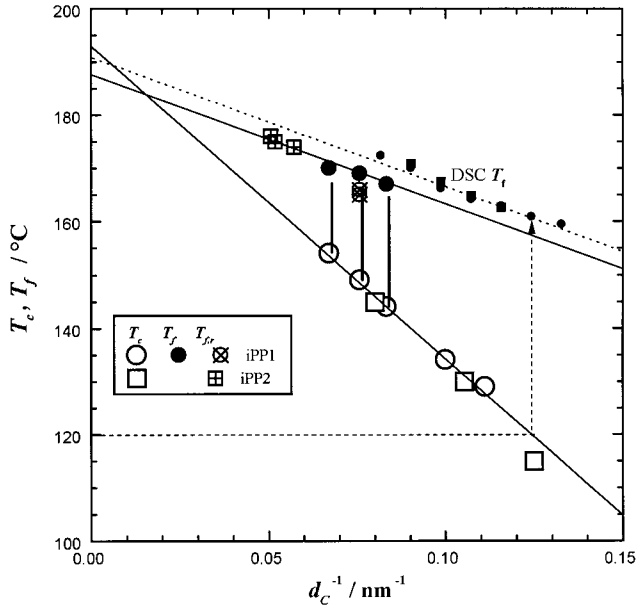

Figure 12. iPP1 and iPP2: relationships T_c vs d_c^{-1} (open symbols, "crystallization line") and T_f vs d_c^{-1} (solid and crossed symbols, "melting line") derived from the SAXS experiments. DSC melting points T_f, plotted under the assumption of a direct melting of lamellae without thickening.

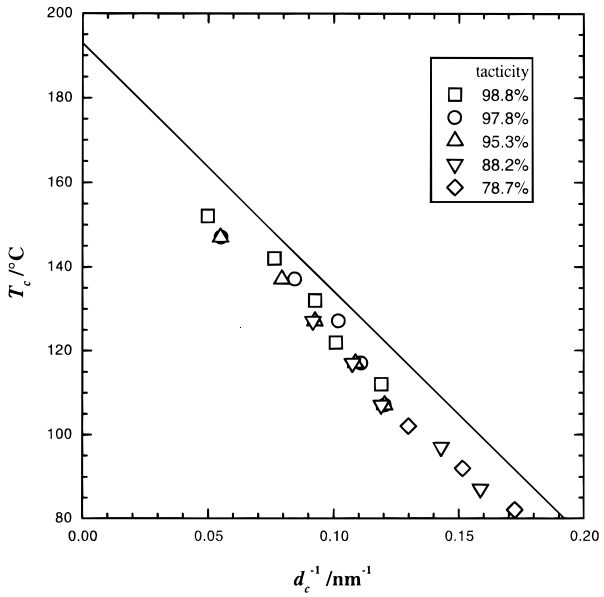

Figure 13. iPPs with various isotacticities: crystal thicknesses after isothermal crystallizations as obtained by Cheng et al.[11] compared to the crystallization line from Figure 12.

thickness d_c^{-1}. This is shown in Figure 12. The open symbols refer to the relation T_c vs d_c^{-1}. As for all other investigated systems, one finds also for isotactic polypropylene a linear dependence, i.e., a crystallization line, and it is the same one for both samples.

We have drawn a certain line, selected by the eye to accommodate a majority of the points but are well aware that due to the low accuracy of the d_c values, the choice is subject to errors. d_c describes the most probable crystal thickness and is therefore well-defined. Its determination, however, is principally difficult in the given case of i-PP, where, as demonstrated by the smeared appearance of $K''(z)$, structure parameters show large fluctuations. As indicated above in the Experimental Section, we tried to reduce the inaccuracy by including into the consideration all three values, d_c, d_a, and L under the condition $d_a + d_c = L$ and additionally the DSC crystallinity. Furthermore, we always commonly looked at all the data obtained during one crystallization and melting experiment. These measures improved the accuracy of the data, but it is difficult to specify the remaining possible deviations. Notwithstanding this problem and seeing the limitations in the determination of the parameter of the crystallization line, the main conclusion is beyond any doubts: there again exists a simple law that controls the crystal thickness.

For syndiotactic polypropylene and derived copolymers the crystallization line was found to be independent of the content of stereodefects and co-units. For isotactic polypropylene we have not got a series of samples that would allow to look again for this property; however, there are data in the literature. Cheng and co-workers carried out experiments on a series of i-PPs with various degrees of isotacticity[11] and thereby determined crystal thicknesses after isothermal crystallizations, using the correlation function approach. Figure 13 shows their results in the way we represent it, as T_c vs d_c^{-1}, in a comparison with the crystallization line of Figure 12. First, one notes that according to Cheng's results also for i-PP, crystal thicknesses are not affected by the content of stereodefects. Apparently authors did not consider this fact as important and did not draw any attention on it. Cheng's data and our crystallization line are in reasonable agreement, considering the error limits and when taking into account that we derived crystal thicknesses from the interface distance distribution function, which gives the most probable value, whereas Cheng and co-workers derived it from the correlation function, which yields the mean value. Hence, it seems to be clear that there is also for isotactic polypropylene a well-defined crystallization line and, furthermore, that it is not affected by the presence of stereodefects.

On the basis of the Gibbs−Thomson law for layerlike crystallites, one expects a linear dependence between the melting temperature T_f and d_c^{-1}. When setting up this melting line, it is necessary to check whether and where melting and recrystallization occurred. For iPP1 there were no such processes for $T_c = 145$ and 155 °C. In the plot this is indicated by the use of vertical lines connecting the two points on the crystallization line with the corresponding ones on the melting line. In the other cases melting−recrystallization occurred in the course of the heating and must be accounted for. The crossed symbols refer to this situation. They indicate locations of melting points T_f together with simultaneously measured values of d_c. All points together define the melting line, and as it turns out, there is no difference between the two samples.

The figure includes also the results of the DSC runs. They were introduced, as is indicated for $T_c = 120$ °C by the broken arrow, under the assumption of a direct melting of the original crystallites grown at T_c. One notes that the DSC data points placed in this way set up a line with the same slope as the SAXS melting line, only being shifted to higher temperatures by 4 °C. This again expresses the previously addressed superheating effect. Further confirmation follows from the literature. A work of Phillips et al.[17] includes measurements of the dependence $T_f(d_c)$, where the crystal thicknesses were derived from measured long spacings in combination

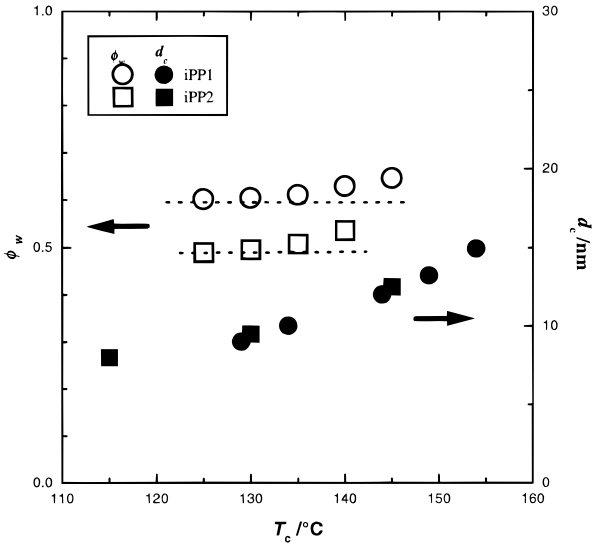

Figure 14. iPP1 and iPP2: crystallinities ϕ_w after isothermal crystallizations at various T_c's determined by DSC. Comparison with the varying values of d_c.

with the crystallinity. Comparison shows that their data perfectly agree with our results (which also implies that the isotacticities were similar to our samples).

In the plot of Figure 12 the crystallization line and the melting line cross each other at a finite d_c; i.e., they do not end at the same limiting temperature for $d_c \rightarrow \infty$. Surely, in the given case it is not possible to state safely that there is a crossing at a finite d_c. However, since for all other investigated systems, s-PP, polyethylene, and poly-ϵ-caprolactone, there was no doubt about this property, one expects it also for i-PP. Of interest is the limiting temperature T_c^∞ of the crystallization line. Both ours and Cheng's data yield $T_c^\infty = 191 \pm 3$ °C. For all systems studied so far T_c^∞ was located at or above the equilibrium melting point of the perfect polymer. It thus sets an upper limit for the equilibrium melting point T_f^∞ of perfect i-PP. Since, furthermore, the latter must be located above the equilibrium melting point of our still imperfect samples, one may set the bounds as 187 °C < T_f^∞(perfect) < 194 °C. In the literature there is still an ongoing discussion about the location of the equilibrium melting point T_f^∞. One finds two groups of values, one around 190 °C and a second one around 210 °C.[1] Our results are clearly in favor of the first choice.

In the studies on the other systems it was generally found that crystallinities when measured at T_c after completion of the crystallization process were essentially constant over the temperature ranges of the studies. The same property holds for i-PP. The data are collected in Figure 14, and the figure includes also the temperature dependence of d_c. One recognizes again that despite larger changes in the length scale of the semicrystalline structure, i.e., in d_c, the changes in the crystallinity remain small. The crystallinity can be varied by changing the isotacticity, the content of co-units, or the molecular weight, but not by the choice of the crystallization temperature. It has to be emphasized that this statement holds for the crystallinities achieved directly at T_c. A successive cooling produces additional secondary crystallites. As a consequence, if crystallinity values are compared at room temperature after isothermal crystallizations at higher temperature, then of course an effect arises.

3.3. WAXS Characterization of Crystal Perfection. Disorder in crystallites has different effects on SAXS data, WAXS diagrams, and DSC heats of melting. One expects the most sensible reaction in the WAXS diagram, where disorder should weaken the integral intensities of the Bragg reflections. Effects on the heats of melting might be less pronounced, and the smallest will be shown by the SAXS curves, as these react to density changes only. We have carried out a comparison and in fact found differences in the temperature dependence of the crystallinity related parameters during heating. Strictly speaking, there is perfect agreement between the changes in the SAXS curves and the enthalpy, as was already observed for s-PP,[7] but one finds deviations when measuring the changes of the intensity of crystal reflections. Comparison between SAXS and WAXS data was carried out as follows. The temperature dependence of the Porod coefficient when corrected for the known temperature dependence of the electron density difference $\Delta\rho_e$[13] yields the temperature dependence of the inner specific surface O_{ca} (eq 6). From the WAXS data we took the integral intensity I of the 110 reflection, after an empirical separation from the diffuse scattering of the amorphous parts. To account for possible changes in the scattering volume, we always determined the integral scattering over the total range of reciprocal space covered by the measurement and corrected I correspondingly if changes were detected. Comparison between $O_{ca}(T)$ and $I(T)$ was carried out as shown in Figure 15. Data refer to a heating of iPP1 after an isothermal crystallization at 145 °C, conducted in both cases with a similar rate on the order of 0.1 K min^{-1}. For comparison, each set of data was referred to the respective value measured at T_f; i.e., the plot shows the two ratios $O_{ac}(T)/O_{ac}(T_f)$ and $I(T)/I(T_f)$. Choosing this representation is based on the assumption that the melting of the lamellar crystallites at T_f would produce equal signals. The lower part of the figure gives in addition the differential quantities, thus providing curves analogous to the DSC thermogram. One recognizes that the two main peaks indeed have the same shape and can be exactly adjusted. On the low-temperature side of the main peak, however, there remains a difference. The melting of the less stable fraction of the crystallites has a weaker effect on the WAXS intensity than on the SAXS data. Figure 16 gives the comparison between the DSC data and the WAXS results. Both curves refer to a higher heating rate, 10 K min^{-1}. Here, the WAXS data were obtained in a run at the HASYLAB, which enables measurements at that higher heating rate to be conducted. The result of the comparison is similar as in Figure 15. One notes again a clear difference at lower temperatures. Analogous measurements were carried out for $T_c = 135$ °C, with similar results. Figure 17 shows the comparison between the SAXS and WAXS data. Again a difference arises on the low-temperature side. The recrystallization after melting shows up in both measurements. Therefore, there are indications that the crystallites of lower stability, melting at lower temperatures, have a higher degree of internal disorder.

3.4. Varying Crystal Stabilities. When heating after an isothermal crystallization melting begins immediately above T_c, i.e., near to the crystallization line, and then extends up to T_f, i.e., to the melting line. One finds either a simple melting without any change in d_c or repeated melting−recrystallization processes char-

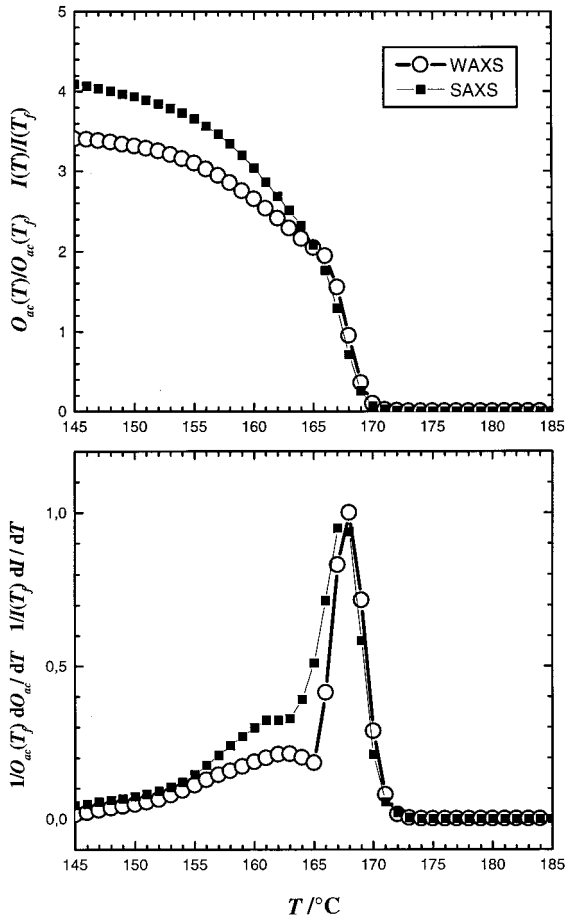

Figure 15. iPP1, crystallized at 145 °C followed by a heating to the melt with a rate of about 0.1 K min^{-1}: comparison of the changes of the inner surface O_{ac} and the intensity I of the 110 reflection. Boths parameters are referred to the values at T_f.

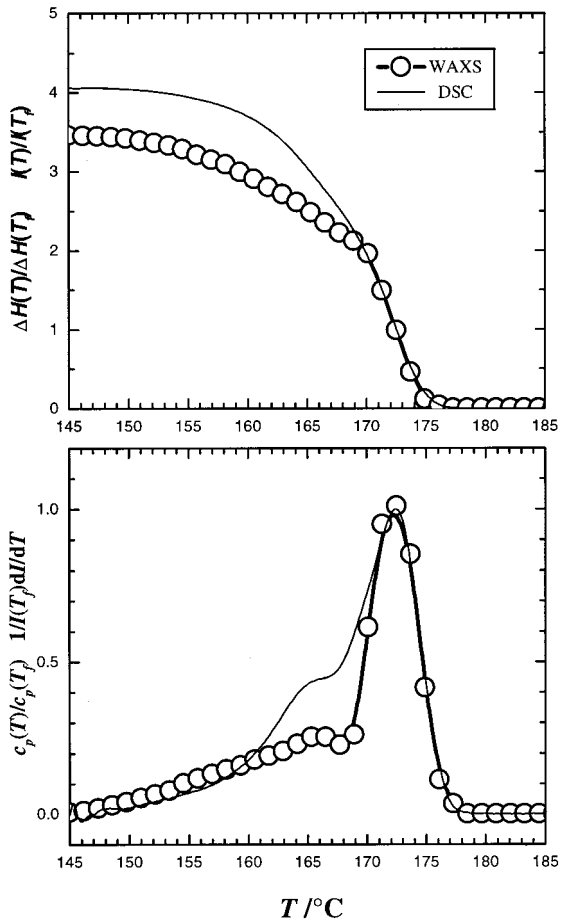

Figure 16. iPP1, crystallized at 145 °C followed by a heating to the melt with 10 K min^{-1}: comparison of the changes of the enthalpy of crystallization and the intensity I of the 110 reflection. Boths parameters are referred to the values at T_f.

acterized by steplike changes in the crystal thickness. A simple melting is typically found after crystallizations at high T_c's; occurrence of melting recrystallization processes is typical for isothermal crystallizations at low T_c's. In general, a sample of i-PP incorporates three kinds of crystallites: (i) the dominant crystallites growing in radial direction at the begin of the transformation process; (ii) "subsidiary" crystallites, also oriented along the radius of the spherulites, forming subsequently by insertion; and (iii) crystallites oriented with their surfaces in the transverse direction, thus producing the characteristic crosshatch morphology. According to the SAXS experiments, the transverse crystallites have the lowest stability. It is the peak around 4 nm in the interface distance distribution function which disappears at first, already at temperatures near to T_c. This agrees with observations of other authors in the optical microscope, for example, recent ones by Alamo et al.[6] Next, the subsidiary radial lamellae melt and at the end then finally the dominant radial lamellae. The three ranges of melting showing up in Figure 3 may therefore be assigned to these three groups of lamellae, i.e., the first range up to 155 °C to the removal of the few transverse crystallites, the next range up to 165 °C with the broad low-temperature endotherm to a melting of the subsidiary radial lamellae, and the final main melting peak to the melting of the dominant radial lamellae.

A straight assignment of the different features in the melting curves for the lower T_c's is not possible. The SAXS experiments show that the structure as a whole has a much reduced stability. For the low heating rate realized in the SAXS experiments the crystallites originally grown at T_c apparently do not reach the melting line but change before by melting−recrystallization processes. As always for melting−recrystallization processes, heating rates play a decisive role. For the heating rate of the DSC, 10 K min^{-1}, recrystallization seems to be mostly suppressed, so that one has again a simple melting. This is indicated by the position of the main endotherm which, according to Figure 12, is exactly on the shifted melting line.

Experiments show that there is no difference in the thicknesses of the two sorts of radial lamellae. On the other hand, results are not clear and accurate enough to enable the thicknesses of the transverse crystallites to be separately determined. One finds, however, hints in the literature. In works in the group of Mandelkern[6] and Bassett,[15] carried out by TEM, no essential difference was observed between the thicknesses of the two groups of crystallites, at least for not too high temperatures. Even more, Bassett compared the thicknesses of different morphologies, structures emanating from a fiber nucleus, transcrystalline structures starting from a plane, and within the common spherulites and again found for a constant T_c always the same thickness. Hence, as was found for all polymer systems investigated so far, here for i-PP again the crystal thickness represents a characteristic inner length which changes

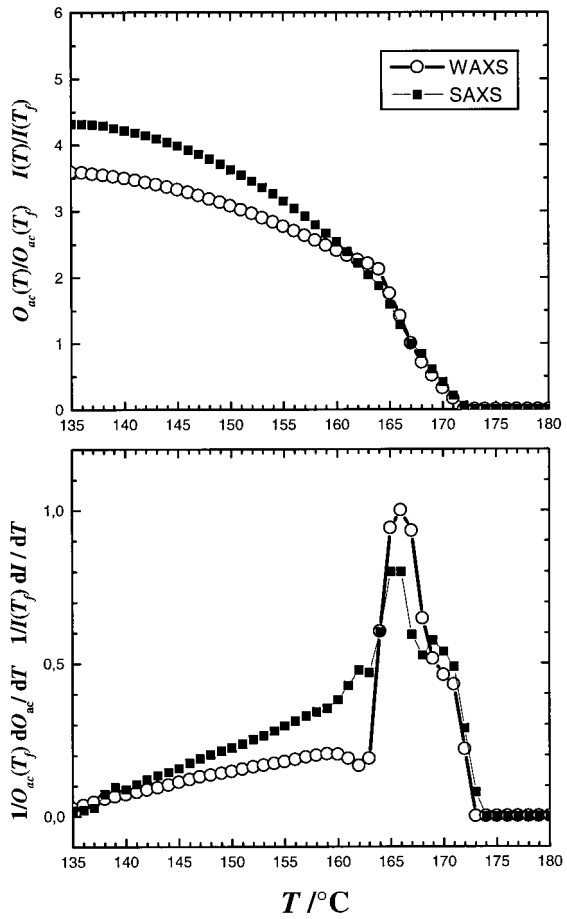

Figure 17. iPP1, crystallized at 135 °C followed by a heating to the melt state: comparison of the changes of the inner surface O_{ac} and the intensity I of the 110 reflection.

only with temperature, and this in a well-defined, simple way.

3.5. On the Nature of the Initial Form and the Way of Its Emergence. Having established the general agreement between the crystallization and melting properties of i-PP and those of s-PP, PE, and PϵCL, we are also led to the same conclusion. Also for i-PP the final state with layer morphology does not evolve from the melt directly but via an intermediate, well-defined initial state of higher free energy. The signature of the initial state is the crystallization line, that of the final state the melting line. Stabilization can be achieved without any measurable change in the crystal thickness, as is demonstrated by the simple melting observed for higher T_c's. Dominant and subsidiary radial crystallites, having the same thickness, both start from the initial form. Whether or not the transverse crystallites follow the same pathway cannot be deduced from our data. If radial and transverse crystallites have indeed similar thicknesses, as is written in the literature, it is also probable.

When asking about the nature of the initial form, we found for the other studied systems numerous indications that it may be described as a planar array of crystal blocks.[8,18,19] Stabilization then is achieved by a fusion of the blocks into continuous layers.[20] Indications came from AFM and TEM studies. So far we did not carry out ourselves comparable experiments for i-PP; however, there are observations in the literature. In a paper by Alamo et al.[6] some of the presented TEM micrographs are addressed as showing a graininess in the lamellae, in particular those obtained for low T_c's and for the transverse daughter lamellae. A granular substructure can also be seen in some of the pictures included in a paper of Yamada et al.[21] Particularly clear is the granular substructure in the AFM patterns shown in a paper of Coulon et al.[22] Hence, there are in fact several observations which suggest that also for i-PP the morphology of the initial form resembles planar arrays of blocks.

The blocks determine with their size in chain direction also the thickness of the final crystal lamellae. The rule that selects the lamellar thickness is therefore identical with the rule that selects the size of the elementary blocks. The latter rule, however, can be directly formulated: Blocks possess that thickness and size which keeps them just stable, for the simple reason that blocks have their melting point more or less immediately above T_c.

Despite the considerable changes in the crystal thickness with T_c and the reported changes in the crosshatch frequency, crystallinities when determined after completion of the crystallization process at T_c show only minor variations, as was already found for the other polymer systems. In a general view these observations suggest that the potential of a given polymer system to crystallize is limited and essentially constant over a larger temperature range. Apparently, crystallization beginning with the formation of the array of blocks proceeds into a melt which is already preordered and thereby has already fixed the achievable crystallinity. There are experiments that lend further support to this view. Light scattering experiments carried out in the group of Inoue[23] demonstrate that prior to the formation of crystallites, at first blocks and then lamellae according to our experiments, a preordering process starts in the melt. Characteristically it does not contribute to the depolarized scattering and can be observed in the polarized light scattering only which would mean that the aggregation results primarily in a densification and no observable birefringence. Apparently, the process is nucleated and then leads to the growth of spheres with a constant growth rate. Light scattering is sensitive enough to detect these features, even if the density difference between the amorphous matrix and the slightly densified spheres is very small. The experiment has now been repeated by Pogodina et al.,[24] with the same results, and these are even more clear because they show a larger distance in time between the beginning of the preordering process and the first appearance of crystallites. When the densified phase covers half of the volume, the crystallinity just starts to rise and is in the order of some percent. Interestingly, simultaneous rheological measurements indicate that it is already the preordering which transfers the melt into a gel. Hence, there are strong indications that the crystal blocks do not evolve from an isotropic quiescent melt but out of a phase that is already preconditioned. Regarding the arrangement of the blocks on planes, one might speculate that the densification observed in Inoue's and Pogodina's experiments follows from the nucleation and growth of layers in the melt which, although noncrystalline, possess some internal order. As one possibility, they might be similar to monolayers of amphiphiles, i.e., composed of straightened sequences in a liquidlike packing. For both isotactic and syndiotactic polypropylene it was observed that crystal thicknesses were not affected by the presence of co-units or stereodefects. The

behavior is conceivable if the formation of the orientationally ordered layers already leads to an exclusion of these defects, because these will always produce a bend and therefore cannot be part of a straightened chain sequence. Of course, at present these are all pure speculations which need experimental confirmation.

4. Conclusion

Coming back to the straight experimental results, these may be summarized as follows. The thickness of the lamellar crystallites in α-form isotactic polypropylene is inversely proportional to the supercooling below a temperature $T_c^\infty = 191 \pm 3$ °C. T_c^∞ is located some degrees above the equilibrium melting point T_f^∞ of the investigated samples, determined by application of the Gibbs−Thomson law. The general behavior with the finding of separate laws governing the crystallization and the melting agrees with similar observations on s-PP, poly(ethylene-*co*-octene)s, and poly-ϵ-caprolactone. It can be understood as indicating that the building up of lamellar crystallites occurs via the formation of a well-defined initial form which then becomes stabilized to end up in the final lamellar crystallites.

Acknowledgment. Support of this work by the Deutsche Forschungsgemeinschaft (Sonderforschungsbereich 428 and Graduiertenkolleg Strukturbildung in Makromolekularen Systemen) is gratefully acknowledged. Thanks are also due to the Fonds der Chemischen Industrie for financial help.

References and Notes

(1) Bicerano, J. *Rev. Macromol. Chem. Phys.* **1998**, *C38*, 391.
(2) Miller, R. L. *Polymer* **1960**, *1*, 135.
(3) Marigo, A.; Marega, C.; Zannetti, R. *Macromol. Chem., Rapid Commun.* **1994**, *15*, 225.
(4) Lotz, B.; Wittmann, J. C. *J. Polym. Sci., Polym. Phys. Ed.* **1986**, *24*, 1541.
(5) Lotz, B. *Polymer* **1998**, *39*, 4561.
(6) Alamo, R. G.; Brown, G. M.; Mandelkern, L.; Lehtinen, A.; Paukkeri, R. *Polymer* **1999**, *40*, 3933.
(7) Hauser, G.; Schmidtke, J.; Strobl, G. *Macromolecules* **1998**, *31*, 6250.
(8) Heck, B.; Hugel, T.; Iijima, M.; Sadiku, E.; Strobl, G. *New J. Phys.* **1999**, *1*, 17.
(9) Huang, T. W.; Alamo, R. G. *Macromolecules* **1999**, *32*, 6374.
(10) Strobl, G. *Acta Crystallogr.* **1970**, *A26*, 367.
(11) Cheng, S. Z. D.; Janimak, J. J.; Zhang, A.; Hsieh, E. T. *Polymer* **1991**, *32*, 648.
(12) Ruland, W. *Colloid Polym. Sci.* **1977**, *255*, 417.
(13) Albrecht, T.; Strobl, G. *Macromolecules* **1995**, *28*, 5267.
(14) Thomann, R.; Wang, C.; Kressler, J.; Mülhaupt, R. *Macromolecules* **1996**, *29*, 8425.
(15) White, H. M.; Bassett, D. C. *Polymer* **1997**, *38*, 5515.
(16) Ryan, A. J.; Stanford, J. L.; Bras, W.; Nye, T. M. *Polymer* **1997**, *38*, 759.
(17) Mezghani, K.; Campbell, R. A.; Phillips, P. J. *Macromolecules* **1994**, *27*, 997.
(18) Magonov, S.; Godovsky, Y. *Am. Lab.* **1999**, *31*, 55.
(19) Loos, J.; Thüne, P. C.; Lemstra, P. J.; Niemantsverdriet, J. W. *Macromolecules* **1999**, *32*, 8910.
(20) Hugel, T.; Strobl, G.; Thomann, R. *Acta Polym.* **1999**, *50*, 214.
(21) Yamada, K.; Matsumoto, S.; Tagashira, K.; Hikosaka, M. *Polymer* **1998**, *39*, 5327.
(22) Coulon, G.; Castelein, G.; G'Sell, C. *Polymer* **1998**, *40*, 95.
(23) Okada, T.; Saito, H.; Inoue, T. *Macromolecules* **1992**, *25*, 1908.
(24) Pogodina, N. V.; Siddiquee, S. K.; van Egmond, J. W.; Winter, H. H. *Macromolecules* **1999**, *32*, 1167.

MA000019M